J. Plasma Phys. (2023), *vol*. 89, 905890502 © The Author(s), 2023.
Published by Cambridge University Press
doi:10.1017/S0022377823000661

Effect of external magnetic field and dust grains on the properties of ion-acoustic waves

K. Deka[1], R. Paul[1], G. Sharma[1], N. Das[1], S. Adhikari[2], R. Moulick[1], S.S. Kausik[1],†, B.K. Saikia[1], O.H. Chin[3] and C.S. Wong[3]

[1]Centre of Plasma Physics, Institute for Plasma Research, Sonapur 782402, Assam, India

[2]Institute for Energy Technology, Instituttveien 8, 2007 Kjeller, India

[3]Department of Physics, Faculty of Science, University of Malaya, 50603 Kuala Lumpur, Malaysia

(Received 11 October 2022; revised 6 June 2023; accepted 27 June 2023)

An experimental study to investigate the effect of an external magnetic field on the propagation of ion-acoustic waves (IAWs) has been carried out in hydrogen plasma containing two-temperature electrons and dust grains. It is a first step in understanding the propagation properties of IAWs in such an environment. A low-pressure hot cathode discharge method is chosen for plasma production. The desired two-electron groups with distinct temperatures are achieved by inserting two magnetic cages with a cusp-shaped magnetic field of different surface field strengths in the same chamber. The dust grains are dropped into the plasma with the help of a dust dropper, which gain negative charges by interacting with the plasma. The IAWs are excited with the help of a mesh grid inserted into the plasma. A planar Langmuir probe is used as a detector to detect the IAWs. The time-of-flight technique has been applied to measure the phase velocity of the IAWs. The results suggest that in the presence of a magnetic field, the phase velocity of IAWs increases, whereas introducing the dust particles leads to the lower phase velocity. The magnetic field is believed to have a significant effect on the wave damping. This study will aid in utilising IAWs as a diagnostic tool to estimate plasma parameters in the presence of an external magnetic field.

Keywords: dusty plasmas, plasma diagnostics, plasma waves

1. Introduction

Ion-acoustic waves (IAWs) are modes of ion oscillations often observed in plasmas. These are low-frequency longitudinal oscillations, which take place with the electrons in the background. These background electrons provide the restoring force essential for the ion oscillations (Hosseini Jenab, Kourakis & Abbasi 2011). The first theoretical prediction of IAWs was reported by Tonks and Langmuir in 1929 (Tonks & Langmuir 1929). Such waves were experimentally observed by Revans in 1933 (Revans 1933) for the first time in a gas discharge tube. The study of IAWs is a very classical area of research in plasma physics, which includes both the linear and nonlinear modes of waves (Mahmood, Mushtaq & Saleem 2003). Thomson in 1933 derived the equation of IAWs using the

† Email address for correspondence: kausikss@rediffmail.com

fluid theory (Thomson & Thomson 1933). Damping of the IAWs is one of its intrinsic properties, classified in two categories *viz.* Landau damping and collisional damping. Out of these, the Landau damping of the IAWs occurs when the electron temperature (T_e) is approximately equal to the ion temperature (T_i). The damping and propagation of the IAWs can easily be studied, if the wave in the plasma is excited using an external source. Wong, Motley & D'Angelo (1964) excited IAWs with the help of a negatively biased grid and consequently studied Landau damping of the waves.

The presence of negative ions in a plasma can have a significant effect on the properties of IAWs. It was observed that when the fraction of negative ions is large, the IAWs split up into two modes, out of which, the faster one undergoes weak Landau damping (D'Angelo & Merlino 1996). Not only this, the pulse velocity of the wave is identical to its phase velocity (Alexeff & Jones 1965). In addition to this, there are instances when two groups of electrons are present in the system, namely the hot and cold. The IAWs are highly responsive to such situations (Sharma *et al.* 2020). The IAWs are also studied in a plasma containing two-temperature electrons. In a two-electron temperature plasma, the electron group with lower energy has the dominant effect on the propagation of IAWs (Jones *et al.* 1975).

In the presence of dust particles, the IAWs get modified as dust ion acoustic waves (DIAWs). The DIAWs propagate in the range of frequencies $kv_{\mathrm{th},i} \ll \omega \ll kv_{\mathrm{th},e}$, where ω, k, $v_{\mathrm{th},i}$ and $v_{\mathrm{th},e}$ are the angular wave frequency, wavenumber, ion thermal velocity and electron thermal velocity, respectively. It has been found that DIAWs travel with higher phase velocity than the usual IAWs (Merlino *et al.* 1997). Barkan, D'Angelo & Merlino (1996) studied DIAWs in a Q-machine, in which it was observed that in the presence of dust grains, the phase velocity of IAWs increases, causing a decrease in the Landau damping. The dispersion relation and rate of Landau damping of DIAWs were derived by a kinetic approach (Hadi & Qamar 2019). Nakamura, Bailung & Shukla (1999) studied linear and nonlinear DIAWs in a homogeneous unmagnetized dusty plasma. The results of the study are significant in the sense that for the linear regime of the wave, the phase velocity and damping increase with the increase in dust density.

Despite a significant number of studies, it is observed that the study of the properties of the IAWs in presence of an external magnetic field is an unexplored area of research. This motivates us to perform this specific study of IAWs in the presence of an external magnetic field. The IAWs are widely used as a diagnostic tool to determine the electron temperature and ion mass of plasma. In addition, they are used to estimate the relative ion concentrations in a two positive ion species plasma, as well as the relative concentration of the negative ions (Hershkowitz & Kim 2008; Saikia *et al.* 2014; Kakati *et al.* 2017). Negative ions are the prime participants for the neutral beam injection in an ITER tokamak. The production of negative ions in plasma involves two methods, volume and surface production. The surface production has better efficiency over the volume process (Kakati *et al.* 2017). It has been established that the density of negative ions increases in the presence of an external magnetic field (Santoso *et al.* 2015). In a low-pressure plasma, a novel surface-assisted volume negative hydrogen ion source has been developed by using caesium (Cs) coated tungsten (W) dust (Kakati *et al.* 2017). The presence of an external magnetic field in these studies may lead to an efficient negative ion source by enhancing the density of the negative ions. As the present study deals with the propagation of IAWs in an external magnetic field, the findings of the study may be helpful to estimate the density of the above-mentioned negative hydrogen source where the presence of magnetic field is essential. This can be a future prospect of the present study.

In this article, we intend to understand the effect of an external magnetic field on the propagation and damping of the linear IAWs. Moreover, the propagation of IAWs depends

https://doi.org/10.1017/S0022377823000661 Published online by Cambridge University Press

on the temperature of the electrons in the plasma. It is a well-known fact that in a plasma with two distinct groups of electrons, the colder electrons have a dominant effect on the IAWs. The effect is prominent even if the plasma contains only 10 % cold electrons. The optical techniques often fail to detect the presence of such cold electrons in the plasma. For those plasmas containing hot electrons as the dominant group, the IAWs acts as a suitable diagnostic tool to determine the presence of cold electrons (Jones *et al.* 1975). Moreover, dust charging study in a two-electron temperature plasma has revealed secondary electron emissions (SEE) from tungsten dust grains (Paul *et al.* 2022). The study shows that the SEE from the dust grains results in an increase in the density of cold electrons, which is expected to have a significant effect on the propagation of IAWs. The present study aims to investigate the role of the two-electron groups on the characteristics of IAWs in the presence of dust and an external magnetic field.

The paper has been organized as follows. In § 2, the production mechanism of the plasma, IAWs excitation and detection have been described. Analysis of the results observed in the experiment is presented and discussed in § 3. The conclusions of the study are drawn in § 4.

2. Experimental set-up

The experimental study of IAWs has been carried out in a cylindrical stainless steel chamber consisting of horizontal and vertical chambers. The experimental chamber looks like an inverted T, as shown in figure 1. The plasma is produced in the horizontal chamber, having a length of 100 cm and a diameter of 30 cm. On the other hand, the vertical chamber is used as the dust dropping unit with a height of 72 cm and a diameter of 15 cm. The chamber is evacuated to a base pressure of 1.5×10^{-5} mbar using a diffusion pump backed by a rotary pump. The working pressure of the hydrogen gas is maintained at 1.7×10^{-4} mbar. A hot cathode filament discharge method has been used to produce the plasma. The primary electrons emitted by the filaments are accelerated by a biasing voltage in the range of 80–90 V, which participate in the ionization of the gas and produce secondary electrons. These secondary electrons are accelerated by the biasing voltage and produce further ionization. Thus, a sustainable discharge condition is achieved. Plasma with two distinct groups of electrons having different temperatures is achieved by inserting two magnetic cages of different surface field strengths (magnetic cage I, 1.2 kG made of strontium ferrite; magnetic cage II, 3.5 kG made of a samarium cobalt) inside the chamber, as depicted in figure 2. Different discharge currents are maintained in the two cages by suitably controlling the filament currents. The discharge current in cage I is fixed at 0.5 A, whereas in cage II it was varied from 1–3 A at a step of 0.5 A. Thus, two different plasmas are produced in the individual cages. The plasmas so produced diffuse at the junction of the two cages, and consequently the plasma at the junction consists of two-electron groups with different temperatures (Sharma *et al.* 2022). The semilogarithmic plot of I–V having two distinct slopes, as displayed in figure 3, confirms the presence of two different electron species with distinguishable temperatures.

The upper and lower slopes give the electron temperatures of cold (T_{ec}) and hot (T_{eh}) components, respectively (Pustylnik, Ohno & Takamura 2006; Pilling & Carnegie 2007).

The effective electron temperature of the plasma is given by (Jones *et al.* 1975)

$$T_{\text{eff}} = n_e T_{ec} T_{eh} / (n_{eh} T_{ec} + n_{ec} T_{eh}), \tag{2.1}$$

where, n_e, n_{ec} and n_{eh} are the total plasma density, density of cold and hot components of the electrons, respectively.

The phase velocity of the IAWs in a two-electron temperature plasma (Jones *et al.* 1975)

https://doi.org/10.1017/S0022377823000661 Published online by Cambridge University Press

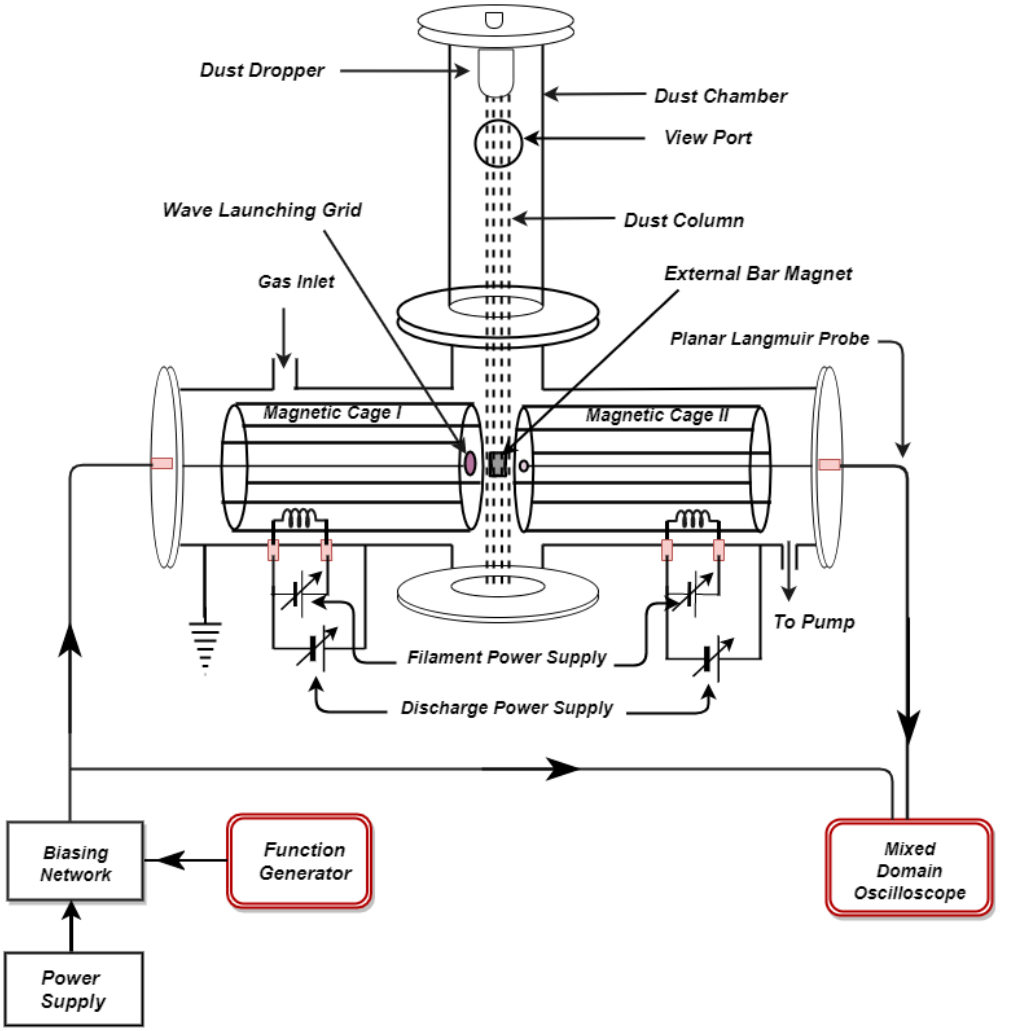

FIGURE 1. Schematic diagram of the experimental set-up.

takes the form

$$\omega/k = \sqrt{k_B T_{\text{eff}}/m_i}, \tag{2.2}$$

where, ω, k, k_B, T_{eff} and m_i are angular frequency, wavenumber, Boltzmann constant, effective electron temperature and mass of the ion, respectively.

In this experiment, the IAWs have been excited by inserting a mesh grid into the plasma column (Wong *et al.* 1964; Barkan *et al.* 1996), which is made of stainless steel, having a diameter of 5 cm with transparency of $\approx 75\,\%$. For appreciable density modulation, the inner-wire spacing of the grid should be comparable to the Debye length and ion gyroradius (Barkan *et al.* 1996; Shukla & Mamun 2001). In the present context, the Debye length and ion gyroradius are ≈ 0.1 mm and 0.115 mm, respectively. Therefore, the inner-wire spacing of the grid is ≈ 0.5 mm, and its surface is perpendicular to the axis of the plasma column. For launching the IAWs, a transistor-based biasing circuit was designed and fabricated, and a sinusoidal voltage, having a frequency in the range of 80–120 kHz with peak-to-peak voltage 4–5 V applied to it. The applied signal creates

https://doi.org/10.1017/S0022377823000661 Published online by Cambridge University Press

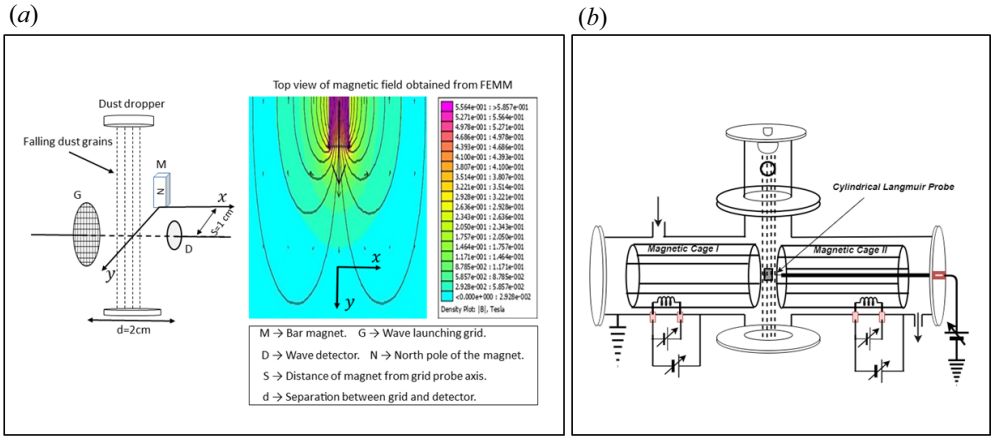

FIGURE 2. (*a*) Relative positions of grid, detector, magnet and dust column along with the magnetic field strength and field lines of the bar magnet. FEMM, Finite element method magnetics. (*b*) Schematic of experimental set-up used for characterization of plasma using cylindrical Langmuir probe.

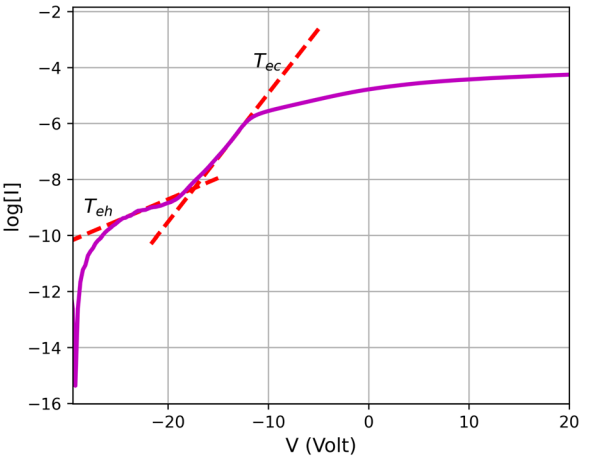

FIGURE 3. Langmuir probe *I*–*V* characteristics in semilogarithmic scale depicting the presence of two-electron temperatures.

a density perturbation, and consequently, it propagates through the plasma as IAWs. A planar Langmuir probe (floating) having a diameter of approximately 9 mm is used to detect the waves. The grid and detector are maintained at a distance of 2 cm from each other. The phase shift and amplitude of the detected waves are measured and recorded with the help of an oscilloscope (MDO3054, 500 MHz). A radially movable bar magnet with a surface field strength of 3.5 kG is introduced into the plasma column in such a way that the magnetic field is perpendicular to the axis of the wave launching grid and the receiver. Figure 4(*a*) describes the magnetic field profile of the external magnet with its position from the grid–detector axis. It can be seen that the magnetic field strength decreases as the magnet is moved away from the axis of the grid and detector.

Dust grains are introduced into the plasma with the help of a dust dropper located at the top of the vertical chamber of the experimental set-up as depicted in figure 1. In the present study tungsten dust with sizes in the range of 2–3 μm has been used. The dust

https://doi.org/10.1017/S0022377823000661 Published online by Cambridge University Press

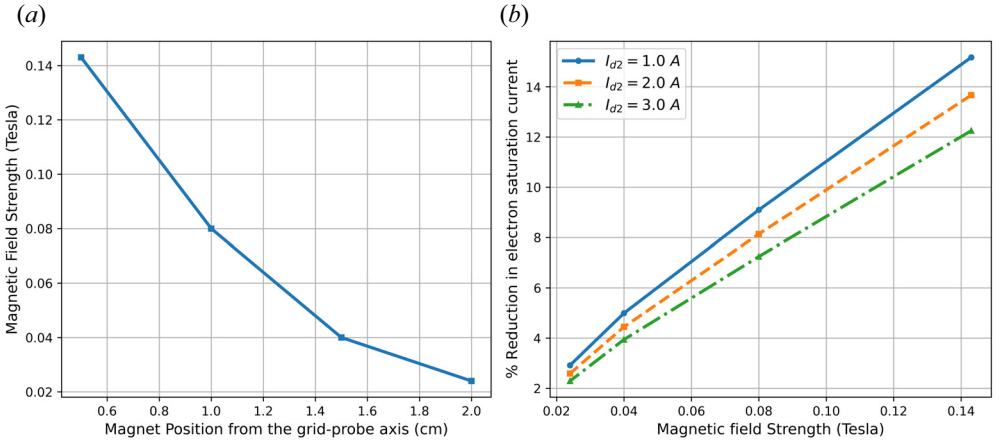

FIGURE 4. (*a*) Magnetic field profile of the external magnet with its position from the grid–detector axis. (*b*) Percentage of reduction in electron saturation current to the cylindrical Langmuir probe in the presence of the external magnetic field for a constant discharge current of $I_{d1} = 0.5$ A in cage I, and a varying discharge currents I_{d2} in cage II.

density is of the order of 10^{11} m^{-3}, which has been obtained using the scattering technique of laser by the dust grains. The amount of scattered laser depends on the density and size distribution of the dust grains. The dust density is determined by the relation

$$I = I_0 \exp(-\eta \pi a^2 l N_d), \tag{2.3}$$

where η is the extinction coefficient, I_0 is the initial laser intensity recorded by the photodiode in the absence of the dust grains, I is the reduced laser intensity when the laser passes through the dust column, l is the width of the dust column and a is the average radius of the dust grains.

For the present study the Havnes parameter $P = Z_d n_d / n_i$ has been found to be less than unity. Therefore, the Havnes parameter does not play a role in the charging of the dust grains. The charge accumulated on the dust grains is estimated with the help of an electrometer (Keithlely 6514) and Faraday cup assembly. The Faraday cup assembly is placed just below the junction of the two cages in such a way that the dust grains falling through the plasma column enter the Faraday cup. To avoid the entry of other charged particles from the plasma into the Faraday cup, a transverse magnetic field is produced in the region of the Faraday cup with the help of two permanent magnets. The electrometer (Keithlely 6514) is connected to the Faraday cup by a low-noise triaxial cable. From the electrometer reading, the charge accumulated on the dust grains has been estimated.

The dust dropper for inserting dust grains into the plasma consists of a cylindrical vessel with a mesh at the bottom surface through which the dust particles fall into the plasma. A direct-current motor is attached to the small dust-containing cylindrical chamber in such a way that whenever the motor rotates, the dust vessel undergoes vibration, and consequently, the dust particles fall through the mesh and enter into the plasma column. These dust grains, in general, acquire a negative charge by interacting with the plasma.

The propagation of the wave is studied in the vicinity of the junction of the two magnetic cages, which also happens to be the central portion of the plasma. A cylindrical Langmuir probe is placed at the middle of the same region of the plasma in the absence of wave launching grid and the detector to determine the plasma parameters. The wave propagation leads to density perturbation in the plasma, considering that factor the plasma

https://doi.org/10.1017/S0022377823000661 Published online by Cambridge University Press

parameters are not estimated simultaneously with the wave propagation. The same plasma conditions have been used for the wave propagation as well as the determination of plasma parameters.

2.1. *Estimation of electron saturation current using Langmuir probe in the presence of an external magnetic field*

The electron current collected by the Langmuir probe is suppressed in the presence of an external magnetic field. The reduction in electron current to the probe is described by the reduction factor r (Stangeby 1982; Tagle, Stangeby & Erents 1987; Pitts & Stangeby 1990),

$$r = 2\lambda_{\mathrm{mfp}} \frac{\sqrt{\alpha}(1+\tau)}{d}, \tag{2.4}$$

where

$$\alpha = D_{\perp}/D_{\parallel} \quad \tau = T_i/T_e. \tag{2.5a,b}$$

Here λ_{mfp} is the momentum loss mean free path of the electrons to the ions; $D_{\perp}$ is the diffusion coefficient perpendicular to magnetic field; $D_{\parallel}$ is the diffusion coefficient parallel to magnetic field; d is the radius of the probe. The reduced value of electron saturation current is given by (Tagle *et al.* 1987)

$$I^e_{\mathrm{sat}} = \frac{1}{4} n_0 e \bar{c_e} A \left(\frac{r}{1+r}\right), \quad \bar{c_e} = \sqrt{\frac{8kT_e}{\pi m}}, \tag{2.6a,b}$$

where, n_0, $\bar{c_e}$ and A are the undisturbed plasma density, random electron thermal velocity and probe area, respectively. However, the ion and electron currents to a floating probe are insensitive to the current reduction factor r, and size of the probe d in the presence of a magnetic field (Stangeby 1982; Stanojević *et al.* 1994). In this work, a planar Langmuir probe at floating potential has been employed for the detection of the IAWs. So, there will be no concern on the validity of the orbital-motion-limited theory for the wave detection in the presence of the magnetic field by the planar Langmuir probe at floating potential. On the other hand, a cylindrical Langmuir probe having a length of 3 mm and diameter of 0.3 mm is used to determine the plasma parameters. The percentage of reduction in electron saturation current, for the present context, in an external magnetic field, for different values of the discharge currents is represented in figure 4(*b*). It is observed that the maximum and minimum value of reduction is approximately 15 % and 2.2 %, respectively. The figure also shows that with the increase of magnetic field strength, the percentage of reduction in electron saturation current increases, but the percentage of reduction decreases with the increase in discharge current.

An attempt has been made to compensate for the reduction in electron saturation current to the cylindrical Langmuir probe in the presence of the magnetic field by adding a correction factor, equivalent to the amount of reduction to the estimated value of current. The corrected value of saturation current has been used to determine the value of the electron density.

2.2. *Estimation of electron temperature using Langmuir probe in the presence of a magnetic field*

Erents *et al.* (1986) and Tagle *et al.* (1987) estimated the value of electron temperature on the plasma boundary of a JET tokamak by applying a nonlinear fit of the form

$$I = I^i_{\mathrm{sat}} \left[1 - \exp\left\{\frac{e(V - V_f)}{kT_e}\right\}\right], \tag{2.7}$$

https://doi.org/10.1017/S0022377823000661 Published online by Cambridge University Press

to the region below floating potential ($V < V_f$), as they found a deviation of the I–V from the exponential behaviour above the floating potential. In such a scenario, the I–V above the floating potential falsely depicts a high electron temperature. In the present work, a similar method as that employed by Erents *et al.* and Tagle *et al.* was tried for the estimation of the electron temperatures, although the I–V in the presence of the magnetic field does not show any discrepancy from the exponential behaviour. However, the method has been found inappropriate for the present context, as it yields electron temperatures that are even much higher than the hot component of the plasma under consideration. Therefore, a different method has been adopted to determine the electron temperature. The first derivative of the I–V is used as the standard method for the evaluation of plasma potential. But, in the presence of a magnetic field, the peak obtained from the first derivative of the I–V is indistinct, leading to some ambiguity in the determination of plasma potential, which is more prominent for a high magnetic field. Hence, this method is also inadequate in the presence of a magnetic field. For such cases, the intersection method is more appropriate for the estimation of plasma potential. The value of plasma potential (V_p), from the semilogarithmic plot of the I–V, is estimated from the intersection of the lines obtained from Usoltceva *et al.* (2018) and Merlino (2007):

(i) extrapolation of the region between floating potential (V_f) and plasma potential (V_p);
(ii) extrapolation of the saturation region of the I–V.

Now, after the correct estimation of the plasma potential, the slope of the linear region between plasma potential (obtained from the intersection method) and floating potential yields the electron temperature.

3. Results and discussion

Figure 5 shows that a distinct phase-shift is observed on changing the separation between the grid and detector, which indeed verifies that a wave has been detected.

3.1. *Variation of phase velocity of IAWs*

Figure 6(*a*) represents the typical waveforms of the applied and the received signals of the IAWs. The phase difference and damping are clearly visible from the figure. Figure 6(*b*) depicts the phase velocity of IAWs observed in a two-electron temperature plasma, which is in the range of 1.38×10^4 m s^{-1} to 3.02×10^4 m s^{-1}. The phase velocity appears to grow as the plasma discharge current increases. The temperature and density of electrons rise with the discharge current as portrayed in figure 7. The increase in electron density tends to provide more shielding to the electric field of the ion bunches, but the subsequent increase in electron temperature reduces the shielding effect. As a result, the phase velocity of the wave will increase.

In a single electron temperature plasma, the phase velocity of the IAWs increases in the presence of dust particles due to the attachment of plasma electrons on the dust grains, which is visible in figure 8(*a*). But in this case, the phase velocity of the IAWs decreases in the presence of dust grains, as shown in figures 6(*b*) and 8(*b*). The justification for it is put forward with the help of figure 7. It shows that in the presence of dust grains, there is a significant rise in the density of the cold component of electrons in a two-electron temperature plasma due to the secondary electron emissions from the dust caused by the combination of primary electrons with energy in the range of 60–80 eV, and hot electron group with energy 10–12 eV (Mamun & Shukla 2003; Paul *et al.* 2022). Besides this, the electron temperature does not change significantly. Due to the rise in density, the shielding of the electric field associated with the bunching of ions increases, and hence

https://doi.org/10.1017/S0022377823000661 Published online by Cambridge University Press

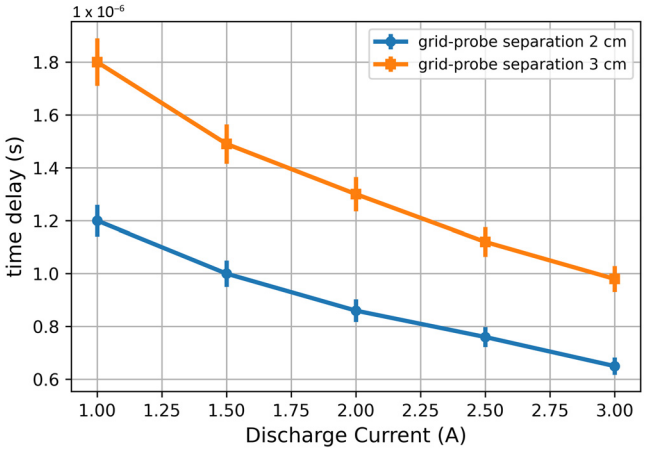

FIGURE 5. Time delay or phase shift between applied and received signal at two different grid–detector separations.

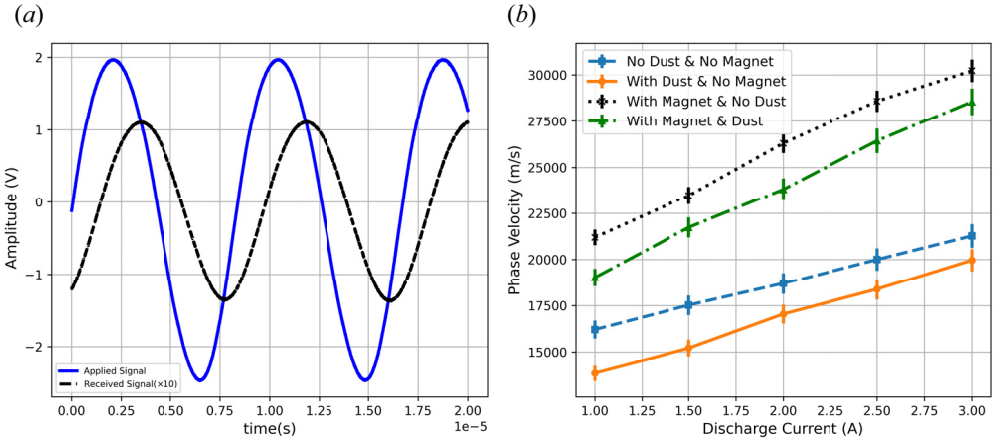

FIGURE 6. (*a*) Waveform of applied and received signal of the wave representing the phase difference and damping. (*b*) Phase Velocity of IAWs at a constant discharge current of $I_{d1} =$ 0.5 A in cage I and different values of discharge currents I_{d2} in cage II.

the phase velocity of the wave decreases. Secondary electron emissions can occur in an environment where the hot electron population is high enough with energy above 10 eV. Such electrons can initiate secondary electron emissions by tunnelling through the dust surface. These electrons lost a part of their energy on striking the dust grains. The lost energy is spent in exciting the electrons on the dust grains, and consequently electrons are emitted from the dust surface. The energy of these emitted electrons is comparable to that of the cold electrons, which leads to the increase in the population of the lower energy electrons (Chow, Mendis & Rosenberg 1993, 1994; Paul *et al.* 2022). The arrangement of the magnetic cages has a contribution in the SEE from the dust grains in the present study. Due to the specific arrangement of the two magnetic cages, the magnetic field lines at the periphery of the junction are almost parallel to the axis of the cylindrical chamber. Hence, the magnetic field at the junction confines the electrons in the central region of the plasma. The field also guides the primary electrons from the filaments towards the junction

https://doi.org/10.1017/S0022377823000661 Published online by Cambridge University Press

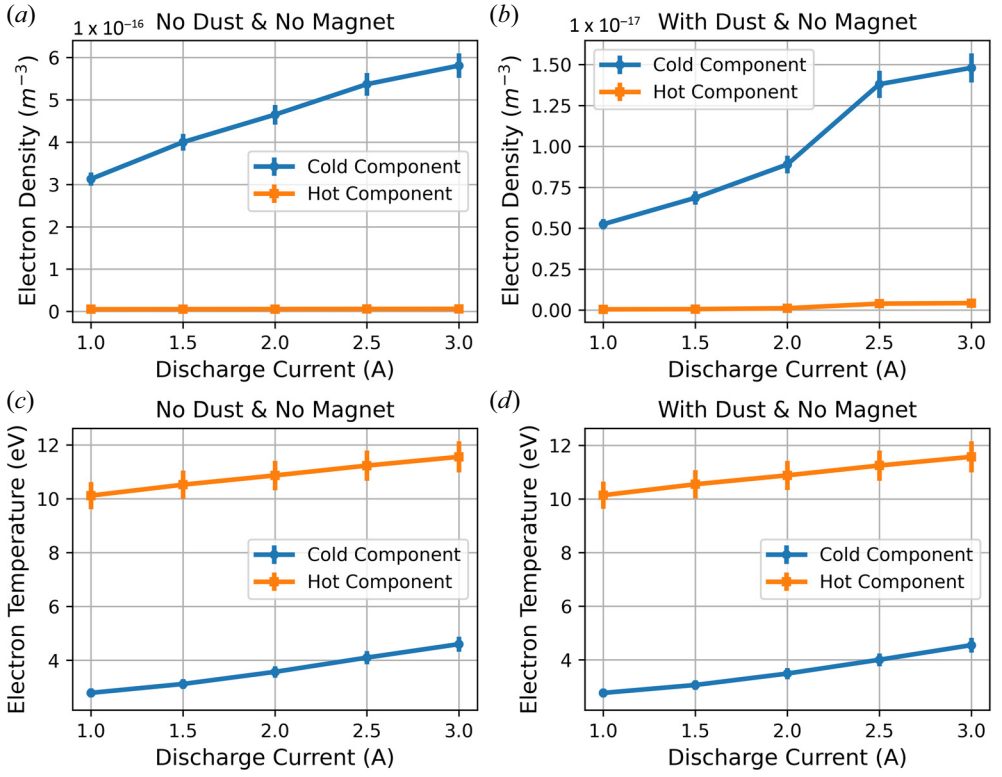

FIGURE 7. (*a*,*b*) Plots of electron densities, and (*c*,*d*) plots of electron temperatures at a constant discharge current of $I_{d1} = 0.5$ A in cage I, and different values of discharge currents I_{d2} in cage II for pure plasma and in the presence of dust particles, respectively.

of the two cages. Therefore, the total electron flux increases significantly at the centre, and consequently, the probability of interaction of these energetic electrons with the dust grains increases, which leads to a sufficient number of secondary electrons emitted from the dust grains (Paul *et al.* 2022).

The secondary electron emissions from the dust grains can also be observed from the *I*–*V* curves (taken with cylindrical Langmuir probe) shown in figure 9. Under normal circumstances, the electron saturation current to the probe drops in the presence of dust grains, indicating that electrons are attached to the dust grains. The electron saturation current can increase only when there are additional electrons in the plasma. The only possible source of these additional electrons, at fixed plasma conditions, is the secondary emissions from the surface of dust grains. Thus, the study of IAWs can be considered as an alternative method for the confirmation of secondary electron emissions from the dust grains in a two-electron temperature plasma that contains high-energetic electrons above 10 eV as we stated in the beginning.

In the presence of an external magnetic field, the electrons participating in the propagation of IAWs may undergo two types of motions depending on the direction of electron velocity: (*a*) cyclotron motion about the field direction; and (*b*) helical motion along the field. The electrons undergoing the cyclotron motion are confined by the magnetic field and are prevented from freely shielding the electric field created by the bunching of ions. Further, the electrons belonging to the helical trajectory are drifted

https://doi.org/10.1017/S0022377823000661 Published online by Cambridge University Press

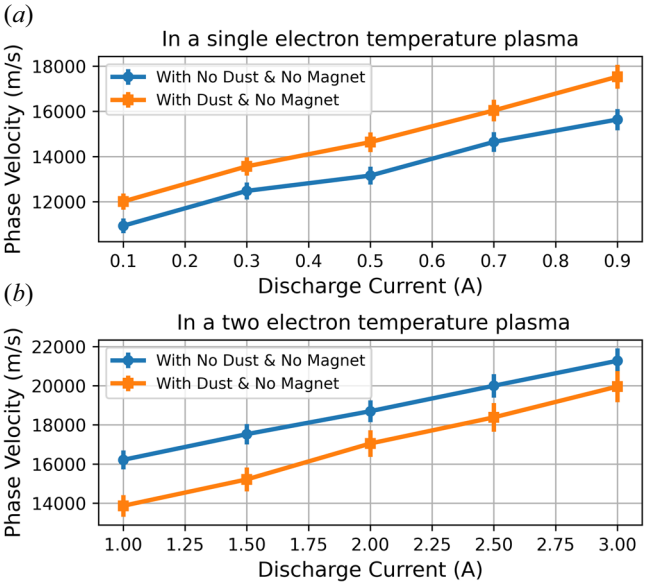

FIGURE 8. (*a*) Phase Velocity of IAWs in a single electron temperature plasma with discharge currents, and (*b*) phase velocity of IAWs in a two electron temperature plasma for a constant discharge current of $I_{d1} = 0.5$ A in cage I and different values of discharge currents I_{d2} in cage II.

away from the wave direction, which as a consequence reduces the number of electrons participating in the shielding process. This subsequently leads to the increase in the phase velocity of IAWs. The dipole field of the bar magnet has some inhomogeneity in the field strength in the region between the wave launching grid and the detector. The field strength is maximum at the middle of the grid–detector axis and decreases gradually on either side. Therefore, the wave experiences an increasing magnetic field up to the axis of the bar magnet. On the contrary, the field strength decreases from the magnetic axis to the detector. The overall effect of the magnetic field is to restrict the movement of the ions and electrons. But, the presence of inhomogeneity of the magnetic field gives rise to gradient drift of the charged particles in the plasma (Deka *et al.* 2021). The gradient of the magnetic field in the region between the grid and magnetic axis is opposite in direction to that of the field gradient between the magnetic axis and detector, and consequently, the gradient drifts of the charged particles are in different directions in the two regions. Irrespective of the direction of the gradient drifts, there is a net loss of electrons and ions participating in the propagation of the wave. The gradient drift of electrons is much higher than the corresponding drift of ions. Therefore, a greater number of electrons are lost than ions. The decrease in electron density reduces the shielding of the electric field and consequently contributes to the increase in phase velocity of the wave. The effective electron temperature increases only slightly in the presence of the magnetic field, and hence cannot play a significant role in the increase in phase velocity. The facts have been depicted in figures 10(*a*) and 10(*b*).

On introducing the dust particles into the plasma, the electrons collide with the dust grains under the effect of the magnetic field. In such collisions, three processes may take place: (*a*) attachment of the electrons on the dust surface; (*b*) scattering of the electrons from the surface of dust; and (*c*) secondary electron emissions from the dust grains. Whenever dust grains are inserted into the plasma, the plasma particles interact with them.

https://doi.org/10.1017/S0022377823000661 Published online by Cambridge University Press

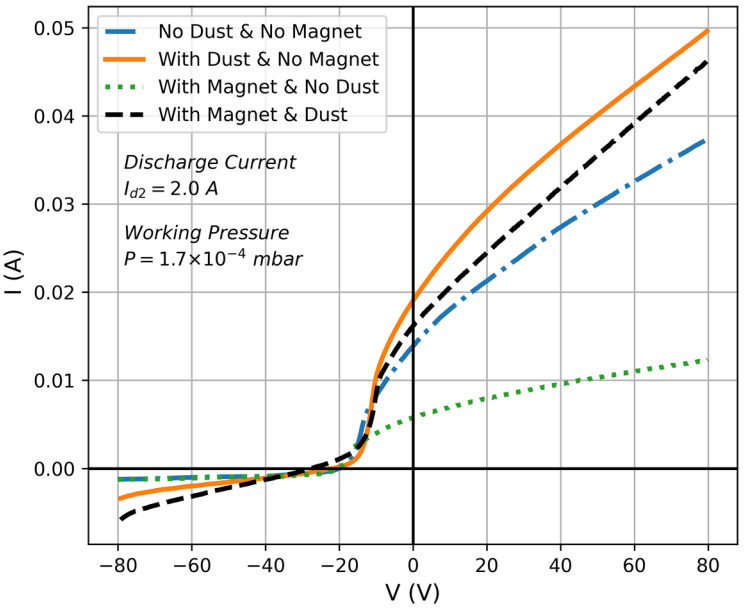

FIGURE 9. Langmuir probe I–V characteristics of plasma at a discharge current of $I_{d1} = 0.5$ A in cage I, and $I_{d2} = 2.0$ A in cage II.

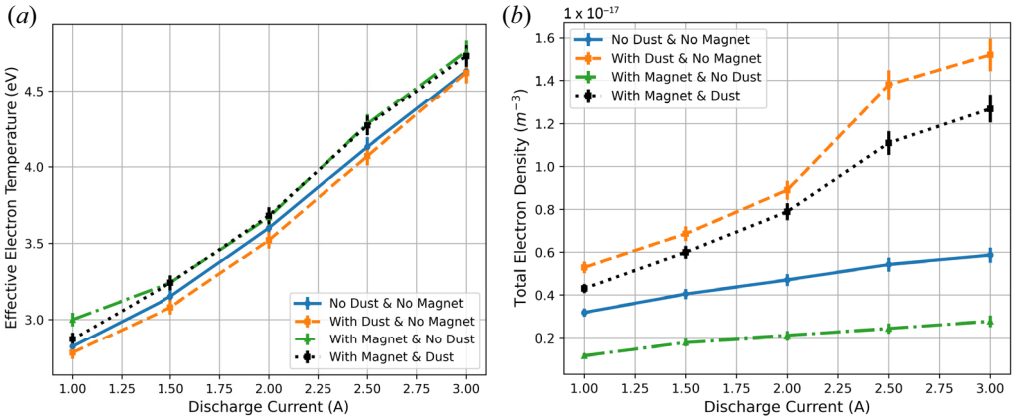

FIGURE 10. (*a*) Effective temperature of electrons for constant discharge current of $I_{d1} = 0.5$ A in cage I and with a variable discharge current I_{d2} in cage II for different environments. (*b*) Total electron density of electrons for constant discharge current of $I_{d1} = 0.5$ A in cage I and with a variable discharge current I_{d2} in cage II for different scenarios.

As a result, the electrons and ions get attached to the dust grains. This process is mainly responsible for the charging of dust grains. The electron attachment on the dust grain will occur even in the presence of a magnetic field. The gyroradius of the electron in this case is greater than the size of the dust particles, which may enhance the scattering of the electrons from the dust and reduce the secondary electron emission from the dust surface by the primary electrons and hot electron component of the plasma. The scattering of the electrons from the dust surface will further lead to two possibilities: (*a*) instantaneous modification of the gyro-orbit of the charged particle; (*b*) restriction of the mobility of

https://doi.org/10.1017/S0022377823000661 Published online by Cambridge University Press

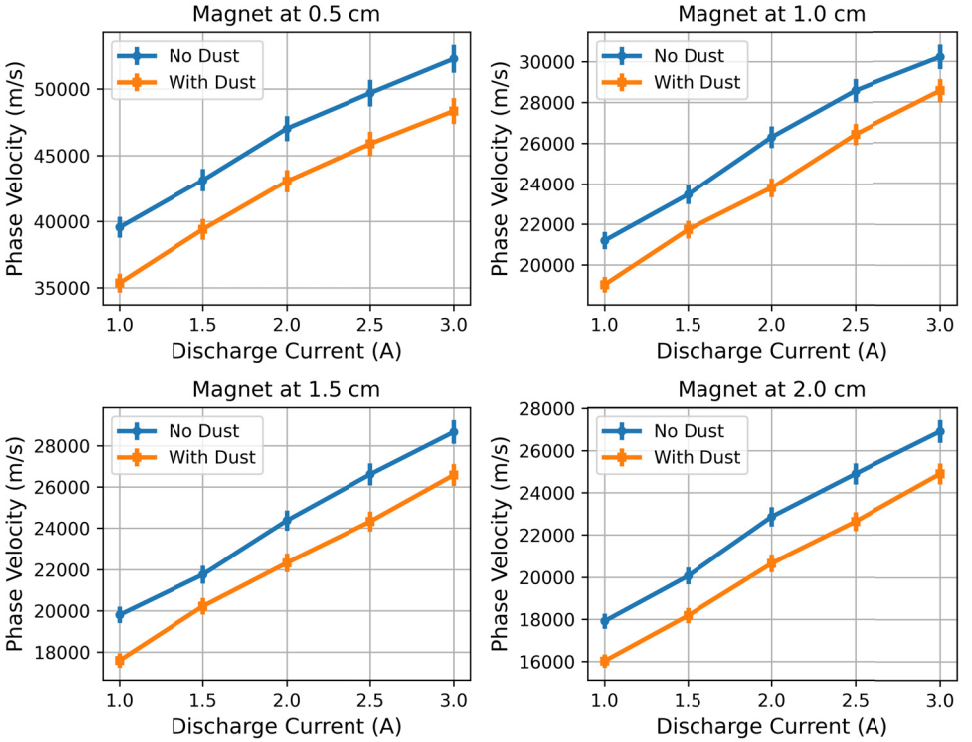

FIGURE 11. Phase velocity of IAWs at different magnet positions with a constant discharge current of $I_{d1} = 0.5$ A in cage I and different values of discharge currents in cage II.

electrons along the field direction. The density of electrons in the presence of dust and a magnet is higher than in the absence of dust (i.e. magnet alone) due to secondary emissions and scattering. There is no significant change in the effective electron temperature in the presence of dust and magnet as depicted in figure 10(*a*). Therefore, this increase in electron density enhances the shielding of the electric field of ion bunches and, hence, the phase velocity decreases.

The phase velocity of IAWs as a function of the discharge current at various magnet positions is depicted in figure 11. It indicates that the phase velocity increases as the discharge current increases, but reduces when dust grains are present. The reason is identical to the one mentioned in the preceding paragraph. It also depicts how the wave phase velocity drop as the magnet is farther away. The strength of the magnetic field at the centre of the plasma column decreases on moving the magnet away from the grid–detector axis. Because of this, the restriction on the movement of the electrons decreases, and the electron density also increases. Consequently, the shielding of the electric field increases, which causes the phase velocity of the wave to decrease. The inhomogeneity of the magnetic field decreases on moving the bar magnet away from the grid–detector axis, which reduces the grad-B drift velocity of the charged particles, and consequently, the phase velocity of IAWs decreases. In this way, the field inhomogeneity contributes towards the phase velocity with magnet position.

https://doi.org/10.1017/S0022377823000661 Published online by Cambridge University Press

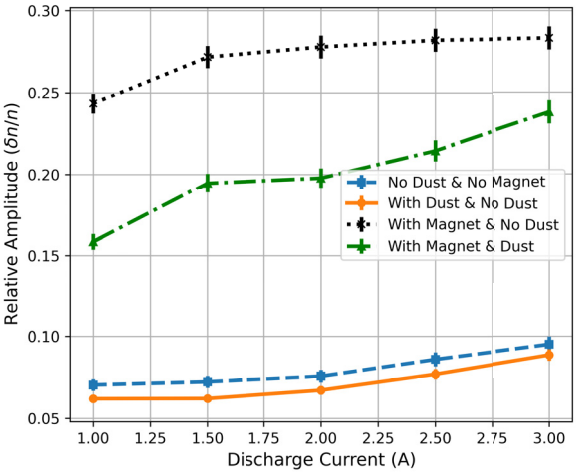

FIGURE 12. Relative wave amplitude of received signal as a function of discharge currents I_{d2} in cage II at a constant discharge current of $I_{d1} = 0.5A$ in cage I.

3.2. *Damping study of IAWs*

The damping of the IAWs can be attributed to either wave–particle interaction known as Landau damping or due to the collision of particles in plasma. Landau damping is dominant in a plasma with ion temperature almost equal to the electron temperature, i.e. $T_i \sim T_e$ (Hosseini Jenab *et al.* 2011). In the present study, $T_e \gg T_i$, so the damping of the wave is collisional. The collisional damping of the IAWs mainly arises from (i) electron–ion, (ii) ion–ion and (iii) ion–neutral collisions (Andersen *et al.* 1968; Buti 1968). In the presence of dust grains, the ion–dust collisions are crucial in the damping of the wave (Nakamura & Bailung 1999).

Figure 12 shows the relative amplitude of the received signal with discharge current. The amplitude of the received signal is normalized by the amplitude of the applied signal. The figure portrays that the damping of the wave decreases with the increase of discharge current. The plasma discharge current increases due to more and more ionization, which causes the neutral density to decrease at a constant pressure. It reduces the collision frequency of ions and electrons with the neutral background. So, the temperature of the ions and the electrons should increase. From the experimental data, it has been observed that the electron temperature increases with the discharge current. Following the same justification, it may be assumed that ion temperature will also increase slightly. As the electron and ion temperature rises, the electron–ion and ion–ion collisions (coulomb collision) will reduce. Hence, the collisions responsible for the damping of the IAWs will decrease, and consequently, the damping will be less.

The damping of the wave will further enhance when dust grains are introduced into the plasma. This additional damping can be attributed to ion–dust collisions. On placing the external magnetic field in the absence of the dust grains, the damping of the wave reduces significantly. The curvature of the charged particle cannot affect the electron–ion collisions if the Larmor radius of electrons (r_{Le}) is approximately equal to the Debye length (λ_D), and the electron cyclotron frequency (Ω_e) is of the order of the electron plasma frequency (ω_e) (Geller & Weisheit 1997). In the present scenario, $r_{\mathrm{Le}} \approx \lambda_D$ and $\Omega_e \approx \omega_e$, which suggest that the magnetic field strength used in this study cannot affect the electron–ion collisions. The gyroradius of the ions (r_{Li}) is greater than the electron gyroradius (r_{Le}), consequently

https://doi.org/10.1017/S0022377823000661 Published online by Cambridge University Press

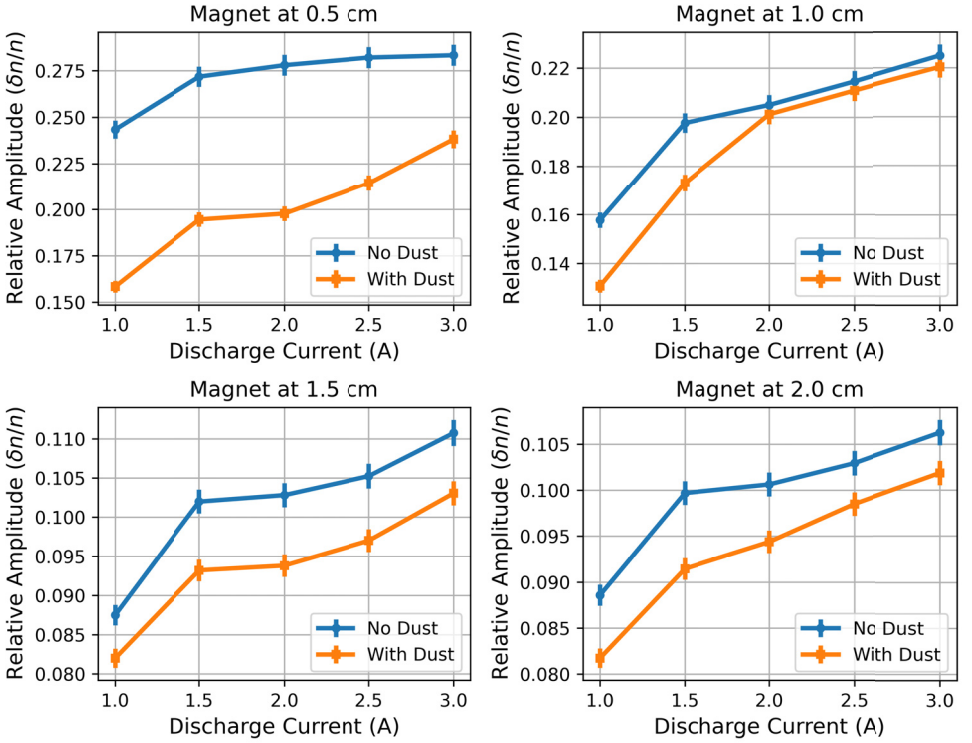

FIGURE 13. Relative amplitude of wave at different magnet positions as a function of discharge currents I_{d2} in cage II keeping the discharge currents in cage I at a constant value of $I_{d1} = 0.5$ A.

the curvature of the ion's trajectory is smaller than the electron's trajectory, which should not affect the ion–ion collisions either. On the contrary, the presence of the magnetic field will reduce the ion–neutral collision frequency (Imazu 1981), which in turn reduces the damping of IAWs. Due to the inhomogeneity of the magnetic field, there is a drift of electrons and ions from the plasma that are participating in the propagation of the wave. The grad-B drift velocity of electrons is much larger than the corresponding drift velocity of ions. Therefore, the rate of loss of electrons is much higher than the rate of loss of ions. The ions take away energy from the wave, hence contributing to the damping of the wave. On the other hand, the loss of electrons reduces the electron–ion collisions, which tends to reduce the damping of the wave. The dampening of the wave increases when dust particles are introduced while the magnetic field is still present in the system.

Figure 13 shows the relative wave amplitudes of the received signal for various values of discharge currents at different magnet positions. It appears that the damping decreases with the increase of discharge current, and with the introduction of dust particles, the damping enhances. It also depicts that the damping increases on moving the magnet away from the grid–detector axis. Imazu (1981) has shown that for magnetic field strength, in the range of 1.5 kG to 0.1 kG, the ion–neutral collision frequency increases almost linearly. The effective field strength for this study varies from 1.43 kG to 0.24 kG, which lies within the range discussed above, consequently the ion–neutral collision increases followed by the damping.

https://doi.org/10.1017/S0022377823000661 Published online by Cambridge University Press

4. Conclusions

The effect of the external magnetic fields on the characteristics of the IAWs in a two-temperature hydrogen plasma has been investigated. The magnetic field has a considerable impact on the propagation and dampening of IAWs.

(1) The presence of a magnetic field in a direction perpendicular to the propagation of IAWs enhances the phase velocity and reduces the damping of the IAWs. The phase velocity increases due to the restriction on the movement of electrons and the reduction of electron density. The electron density decreases because of the diffusion along the field direction. As a result, the electric field generated by the ion bunches is less shielded. The damping is weakened owing to the decrease of ion–neutral collisions in the presence of the magnetic field.
(2) The wave phase velocity is lower in the presence of the magnetic field and dust particles than it is when the magnetic field is present alone, which is due to secondary emissions and scattering of the electrons from the dust grains.
(3) When the magnet is gradually moved away from the grid detector axis, the damping of the waves increases, but the phase velocity decreases. The damping grows as the ion–neutral collisions increase with the lowering of the field strength. On the contrary, the restrictions on the movement of the electrons decrease, and electron density also increases with the reduction of the field strength. Due to this, the shielding of the electric field associated with the ion bunches increases, and consequently, the phase velocity decreases.
(4) When dust particles are introduced in the plasma in the absence of a magnetic field, the phase velocity of the IAWs decreases. The secondary electron emission from the tungsten dust, caused by the energetic group of electrons, in the range of 10–12 eV is responsible for the reduction in velocity. This phenomenon is possible only if there are energetic groups of electrons in the plasma.
(5) The damping of the wave in the presence of dust grains increases for all the plasma environments explored in the present study. This damping is directly associated with ion–dust collisions.

In the presence of the external magnetic field, the ion–neutral collisions seem to be responsible for the change in damping of the wave. Therefore, from the damping of the IAWs, it may be possible to determine the ion–neutral collision frequency. The study can be used to confirm the secondary emissions of electrons from dust grains in a two-electron temperature plasma. The results of this study will be helpful for using IAWs as a diagnostic tool for probing plasma parameters in the presence of a magnetic field. It is worth mentioning that the results obtained are independent of the present experimental set-up. Such observations can be replicated in any experimental system containing two-electron groups with different energies. The next step of the study will be to create a theoretical model to determine the dispersion relation of the IAWs and eventually describe the current findings.

Acknowledgements

The authors would like to thank Mr G.D. Sarma, and Mr S. Zaman for their technical help during the experiment.

Editor E. Thomas, Jr. thanks the referees for their advice in evaluating this article.

Declaration of interest

The authors report no conflict of interest.

Funding

This research received no specific grant from any funding agency, commercial or not-for-profit sectors.

Data availability statement

The data that support the findings of this study are available from the corresponding author upon reasonable request.

REFERENCES

ALEXEFF, I. & JONES, W.D. 1965 Collisionless ion-wave propagation and the determination of the compression coefficient of plasma electrons. *Phys. Rev. Lett*. **15**, 286–288.

ANDERSEN, H.K., D'ANGELO, N., JENSEN, V.O., MICHELSEN, P. & NIELSEN, P. 1968 Effects of ion-atom collisions on the propagation and damping of ion-acoustic waves. *Phys. Fluids* **11** (6), 1177–1180.

BARKAN, A., D'ANGELO, N. & MERLINO, R.L. 1996 Experiments on ion-acoustic waves in dusty plasmas. *Planet. Space Sci*. **44** (3), 239–242.

BUTI, B. 1968 Ion acoustic waves in a collisional plasma. *Phys. Rev*. **165** (1), 195.

CHOW, V.W., MENDIS, D.A. & ROSENBERG, M. 1993 Role of grain size and particle velocity distribution in secondary electron emission in space plasmas. *J. Geophys. Res.: Space Phys*. **98** (A11), 19065–19076.

CHOW, V.W., MENDIS, D.A. & ROSENBERG, M. 1994 Secondary emission from small dust grains at high electron energies. *IEEE Trans. Plasma Sci*. **22** (2), 179–186.

D'ANGELO, N. & MERLINO, R.L. 1996 Current-driven dust-acoustic instability in a collisional plasma. *Planet. Space Sci*. **44** (12), 1593–1598.

DEKA, K., ADHIKARI, S., MOULICK, R., KAUSIK, S.S. & SAIKIA, B.K. 2021 Effect of collisions on the plasma sheath in the presence of an inhomogeneous magnetic field. *Phys. Scr*. **96** (7), 075606.

ERENTS, S.K., TAGLE, J.A., MCCRACKEN, G.M., STANGEBY, P.C. & DE KOCK, L. 1986 Probe measurements of the density and temperature profiles in the jet plasma boundary. *Nucl. Fusion* **26** (12), 1591.

GELLER, D.K. & WEISHEIT, J.C. 1997 Classical electron-ion scattering in strongly magnetized plasmas. I. A generalized coulomb logarithm. *Phys. Plasmas* **4** (12), 4258–4271.

HADI, F. & QAMAR, A. 2019 Kinetic study of dust ion acoustic waves in a nonthermal plasma. *J. Phys. Soc. Japan* **88** (3), 034501.

HERSHKOWITZ, N. & KIM, Y.-C.G. 2008 Probing plasmas with ion acoustic waves. *Plasma Sources Sci. Technol*. **18** (1), 014018.

HOSSEINI JENAB, S.M., KOURAKIS, I. & ABBASI, H. 2011 *Phys. Plasmas* **18** (7), 073703.

IMAZU, S. 1981 Collision frequency of charged particles in a weekly ionized gas in a strong magnetic field. *Phys. Rev.* A **23** (5), 2644.

JONES, W.D., LEE, A., GLEMAN, S.M. & DOUCET, H.J. 1975 Propagation of ion-acoustic waves in a two-electron-temperature plasma. *Phys. Rev. Lett*. **35**, 1349–1352.

KAKATI, B., KAUSIK, S.S., BANDYOPADHYAY, M., SAIKIA, B.K. & KAW, P.K. 2017 Development of a novel surface assisted volume negative hydrogen ion source. *Sci. Rep*. **7** (1), 1–12.

MAHMOOD, S., MUSHTAQ, A. & SALEEM, H. 2003 Ion acoustic solitary wave in homogeneous magnetized electron-positron-ion plasmas. *New J. Phys*. **5**, 28–28.

MAMUN, A.A. & SHUKLA, P.K. 2003 Charging of dust grains in a plasma with negative ions. *Phys. Plasmas* **10** (5), 1518–1520.

MERLINO, R.L. 2007 Understanding langmuir probe current-voltage characteristics. *Am. J. Phys*. **75** (12), 1078–1085.

MERLINO, R.L., BARKAN, A., THOMPSON, C. & D'ANGELO, N. 1997 Experiments on waves and instabilities in dusty plasmas. *Plasma Phys. Control. Fusion* **39** (5A), A421.

NAKAMURA, Y. & BAILUNG, H. 1999 A dusty double plasma device. *Rev. Sci. Instrum*. **70** (5), 2345–2348.

NAKAMURA, Y., BAILUNG, H. & SHUKLA, P.K. 1999 Observation of ion-acoustic shocks in a dusty plasma. *Phys. Rev. Lett*. **83** (8), 1602.

PAUL, R., SHARMA, G., DEKA, K., ADHIKARI, S., MOULICK, R., KAUSIK, S.S. & SAIKIA, B.K. 2022 Experimental study of charging of dust grains in the presence of energetic electrons. *Plasma Phys. Control. Fusion* **64** (3), 035009.

PILLING, L.S. & CARNEGIE, D.A. 2007 Validating experimental and theoretical langmuir probe analyses. *Plasma Sources Sci. Technol*. **16** (3), 570.

PITTS, R.A. & STANGEBY, P.C. 1990 Experimental tests of langmuir probe theory for strong magnetic fields. *Plasma Phys. Control. Fusion* **32** (13), 1237.

PUSTYLNIK, M., OHNO, N. & TAKAMURA, S. 2006 Control of energetic electron component in a magnetically confined diffusion Ar plasma. *Japan. J. Appl. Phys*. **45** (2R), 926.

REVANS, R.W. 1933 The transmission of waves through an ionized gas. *Phys. Rev*. **44**, 798–802.

SAIKIA, P., SAIKIA, B.K., GOSWAMI, K.S. & PHUKAN, A. 2014 Argon–oxygen dc magnetron discharge plasma probed with ion acoustic waves. *J. Vac. Sci. Technol.* A*: Vac. Surf. Films* **32** (3), 031303.

SANTOSO, J., MANOHARAN, R., O'BYRNE, S. & CORR, C.S. 2015 Negative hydrogen ion production in a helicon plasma source. *Phys. Plasmas* **22** (9), 093513.

SHARMA, G., ADHIKARI, S., MOULICK, R., KAUSIK, S.S. & SAIKIA, B.K. 2020 Effect of two temperature electrons in a collisional magnetized plasma sheath. *Phys. Scr*. **95** (3), 035605.

SHARMA, G., DEKA, K., PAUL, R., ADHIKARI, S., MOULICK, R., KAUSIK, S.S. & SAIKIA, B.K. 2022 Experimental study on controlled production of two-electron temperature plasma. *Plasma Sources Sci. Technol*. **31** (2), 025013.

SHUKLA, P.K. & MAMUN, A.A. 2001 *Introduction to Dusty Plasma Physics*, p. 135. IOP Publishing.

STANGEBY, P.C. 1982 Effect of bias on trapping probes and bolometers for tokamak edge diagnosis. *J. Phys.* D*: Appl. Phys*. **15** (6), 1007.

STANOJEVIĆ, M., ČERČEK, M., GYERGYEK, T. & JELIĆ, N. 1994 Interpretation of a planar langmuir probe current–voltage characteristic in a strong magnetic field. *Contrib. Plasma Phys*. **34** (5), 607–633.

TAGLE, J.A., STANGEBY, P.C. & ERENTS, S.K. 1987 Errors in measuring electron temperatures using a single langmuir probe in a magnetic field. *Plasma Phys. Control. Fusion* **29** (3), 297.

THOMSON, J.J. & THOMSON, G.P. 1933 *Conduction of Electricity through Gases*, Part II, p. 353. Cambridge University Press.

TONKS, L. & LANGMUIR, I. 1929 Oscillations in ionized gases. *Phys. Rev*. **33**, 195–210.

USOLTCEVA, M., FAUDOT, E., DEVAUX, S., HEURAUX, S., LEDIG, J., ZADVITSKIY, G.V., OCHOUKOV, R., CROMBÉ, K. & NOTERDAEME, J.-M. 2018 Effective collecting area of a cylindrical langmuir probe in magnetized plasma. *Phys. Plasmas* **25** (6), 063518.

WONG, A.Y., MOTLEY, R.W. & D'ANGELO, N. 1964 Landau damping of ion acoustic waves in highly ionized plasmas. *Phys. Rev*. **133**, A436–A442.